Sensors and Actuators A 165 (2011) 79–85

Contents lists available at ScienceDirect

Sensors and Actuators A: Physical

journal homepage: www.elsevier.com/locate/sna

Experimental study of the effect of hydrodynamic coupling of micro-cantilever array on the dynamic response of micro-cantilever

Jiunn-Horng Lee[a,c], Yung-Dong Lau[b], Chih-Min Yao[c], Weileun Fang[a,b,*]

[a] Institute of NanoEngineering and MicroSystems, National Tsing Hua University, No. 101, Section 2, Kuang-Fu Road, Hsinchu, Taiwan
[b] Department of Power Mechanical Engineering, National Tsing Hua University, No. 101, Section 2, Kuang-Fu Road, Hsinchu, Taiwan
[c] National Center for High-performance Computing, National Applied Research Laboratories, No. 7, R&D Rd. VI, Hsinchu Science Park, Hsinchu, Taiwan

ARTICLE INFO

Article history:
Available online 4 January 2010

Keywords:
Micro-cantilever array
Quality factor
Air damping
Hydrodynamic force

ABSTRACT

This study experimentally investigates the effect of hydrodynamic coupling of a micro-cantilever array on the dynamic response of a micro-cantilever. The micro-cantilever array consists of three harmonically driven micro-cantilevers dynamically coupled through air flow. The right cantilever and left cantilever (auxiliary-cantilevers) adjacent to the middle cantilever (operating-cantilever) are exploited to generate hydrodynamic force to change the air damping of operating-cantilever. Thus, the quality factor of operating-cantilever can be controlled by changing the phase and magnitude of excitation force on auxiliary-cantilevers, and varying the gap between auxiliary-cantilevers and operating-cantilever. In the experiment, magnetic actuated micro-cantilever arrays were fabricated and characterized. Measurements show the variation of quality factor of operating-cantilever is from −39% to +27%.

1. Introduction

The dynamic behavior of microelectromechanical systems (MEMS) devices is affected by their energy losses during the operation. The mechanisms of dynamic energy dissipation in MEMS devices can be classified as intrinsic losses and extrinsic losses [1,2]. The intrinsic losses arise from the interactions of thin film materials, such as thermoelastic damping, crystallographic defects and surface loss. The extrinsic losses, including air damping (slide-film, squeeze-film and free space) and clamping loss, result from the interactions of MEMS devices with the environment. The quality factor Q defined as the ratio of the energy stored to the energy dissipated per cycle is commonly employed as an indicator to characterize the dynamic response of MEMS devices [3,4]. Since the dynamic performances, such as sensitivity, resolution, and response time, of MEMS biosensor [5], chemical sensor [6], scanning probe microscope (SPM) [7], pressure sensor [8], mass sensor [9], viscosity sensor [10] and micromirror [11] are closely related to their quality factors, it is of useful to tune the quality factor of MEMS devices to further control their dynamic performances.

As MEMS devices operate at atmosphere pressure, air damping is the dominant factor for energy losses and changes the dynamic behavior of MEMS devices dramatically [12,13]. Therefore, the approaches to control the dynamic response of MEMS devices using air-damping effects have been extensively investigated. In general, the controlling techniques can be categorized as: passive control and active control. The passive approaches exploit squeeze-film damping [14], slide-film damping [15], and variations of geometry [16] to control the quality factor of the dynamic system. However, these approaches are less effective in increasing the quality factor. The active approach adopts the Q-control [17–19] method to control the dynamic characteristics of microstructures. Although the Q-control method can effectively control the dynamic response of MEMS devices, it needs complicated electronic feedback circuits with a phase-shifter and amplifier to increase or decrease the quality factors of MEMS devices.

On the other hand, Hosaka and Itao [20] studied the coupled vibration of micro-cantilever array and suggested the vibration-induced air flow could be applied to improve the dynamic performance of microstructures. Thus, this study quantitatively evaluates the effect of hydrodynamic coupling of a micro-cantilever array on the quality factor of a micro-cantilever by experiment. In the experiment, micro-cantilever arrays consisting of three cantilevers driven by harmonic Lorenz force have been fabricated and characterized. The cantilever located in the center of a micro-cantilever array, named operating-cantilever, is employed for some particular applications. The rest of the two cantilevers (named

* Corresponding author at: Department of Power Mechanical Engineering, National Tsing Hua University, No. 101, Section 2, Kuang-Fu Road, Hsinchu, Taiwan. Tel.: +886 3 574 2923; fax: +886 3 573 9372.
E-mail address: fang@pme.nthu.edu.tw (W. Fang).

0924-4247/$ – see front matter © 2009 Elsevier B.V. All rights reserved.
doi:10.1016/j.sna.2009.12.024

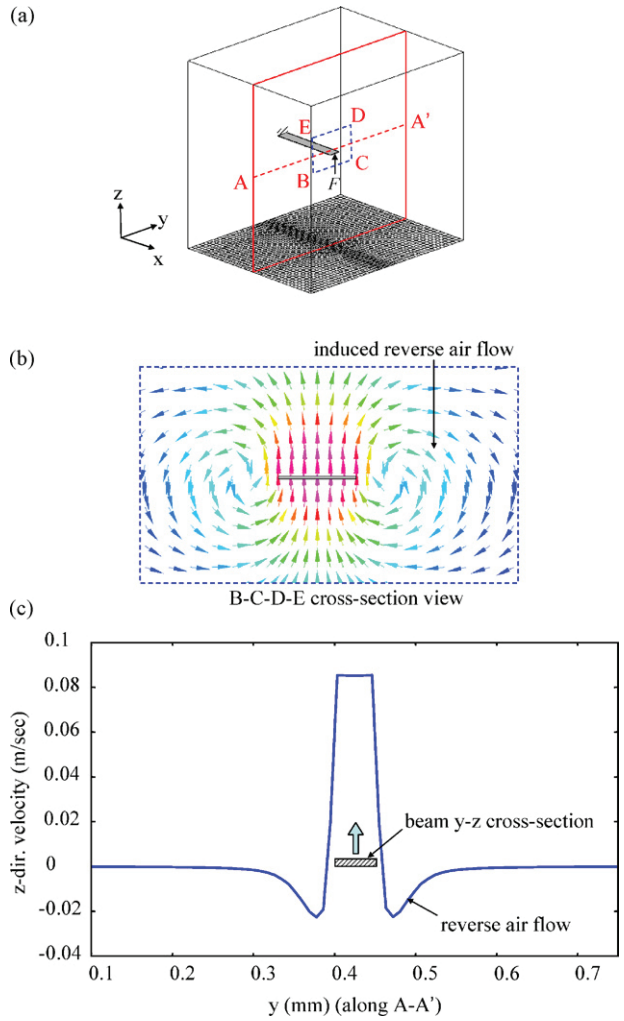

Fig. 1. The hydrodynamic effect of a vibrating cantilever by numerical simulation, (a) the numerical model, (b) simulated air velocity field at the cross-section area of B–C–D–E, and (c) velocity profile along the cross-sectional line of A–A′.

auxiliary-cantilevers) are exploited to generate velocity-dependent hydrodynamic force on operating-cantilever. Thus, the quality factor of operating-cantilever can be tuned by controlling the oscillation of auxiliary-cantilevers.

2. Analysis

This study employs the commercial software *CFD-ACE+* to simulate the hydrodynamic coupling of micro-cantilevers [21]. The numerical simulation provides the insight of fluid structure interaction, which facilitates the design of experiment. Fig. 1 shows a typical hydrodynamic effect resulted from a vibrating SiO_2 cantilever with a length of 300 μm, width of 50 μm, and thickness of 1.68 μm by numerical simulation. Fig. 1(a) shows the numerical simulation model consisting of the cantilever and its surrounding air. Thus, the dynamics as well as dynamic coupling of cantilever and air can be predicted. Fig. 1(b) indicates the magnitude and direction of air velocity at the cross-section area of B–C–D–E depicted in Fig. 1(a) using the arrows (arrow shows the direction, and color represents the magnitude). Fig. 1(c) quantitatively shows the variation of the velocity profile along the cross-section line of A–A′ indicated in Fig. 1(a). As indicated in Fig. 1(b) and (c), the vibrating micro-cantilever induces reverse air flow in both left-hand and right-hand sides of beam, and will generate hydrodynamic force to its adjacent microstructures. Therefore, as various

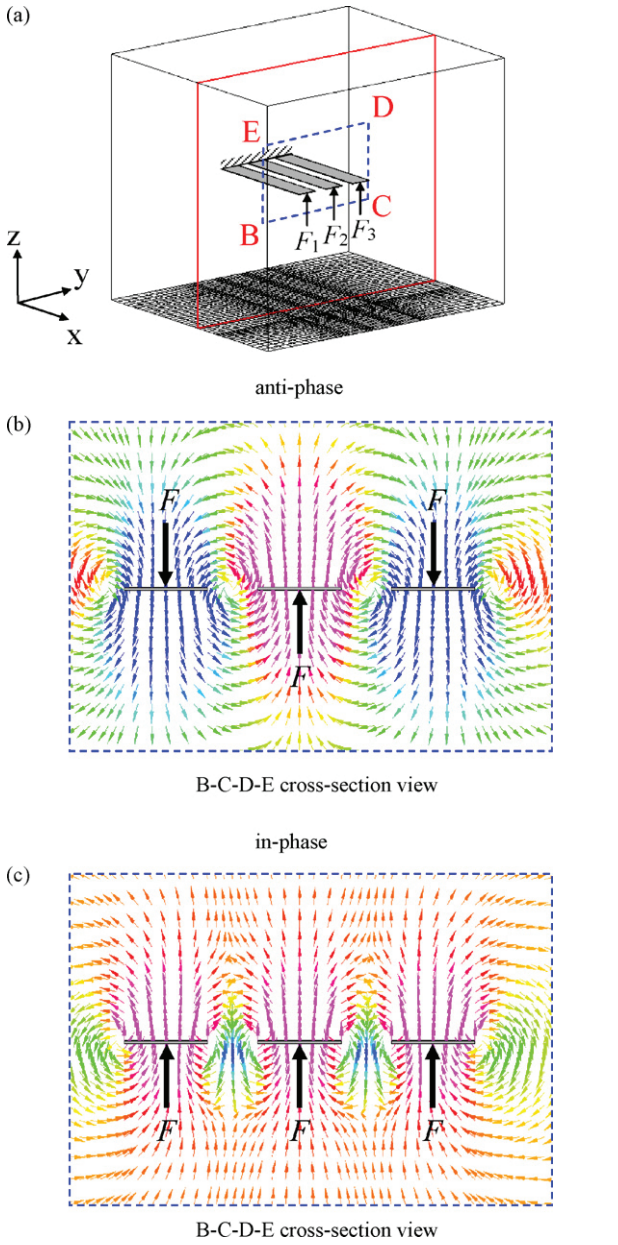

Fig. 2. The hydrodynamic coupling effect of micro-cantilever array by numerical simulation, (a) the numerical model, (b) simulated air velocity field at the cross-section area of B–C–D–E (anti-phase), and (c) simulated air velocity field at the cross-section area of B–C–D–E (in-phase).

micro-cantilevers are adjacent to each other, these beams will be dynamically coupled by the vibration-induced air flow. Thus, this brings up the study to employ the hydrodynamic coupling effect to control the dynamic characteristics of a micro-cantilever using the micro-cantilever array.

Fig. 2 shows a typical design of the micro-cantilever array consisted of three identical cantilevers. Fig. 2(a) shows the numerical simulation model of the micro-cantilever array with a gap of 30 μm between cantilevers. The three micro-cantilevers are driven by harmonic forces F_1, F_2, and F_3, respectively. The simulation results in Fig. 2(b) and (c) further show the typical hydrodynamic coupling of the three micro-cantilevers while vibrating in anti-phase and in-phase, respectively. Fig. 2(b) and (c) indicates the magnitude and direction of air velocity at the cross-section area of B–C–D–E depicted in Fig. 2(a) using the arrows (arrow shows the direction, and color represents the magnitude). Fig. 3 shows the numerical

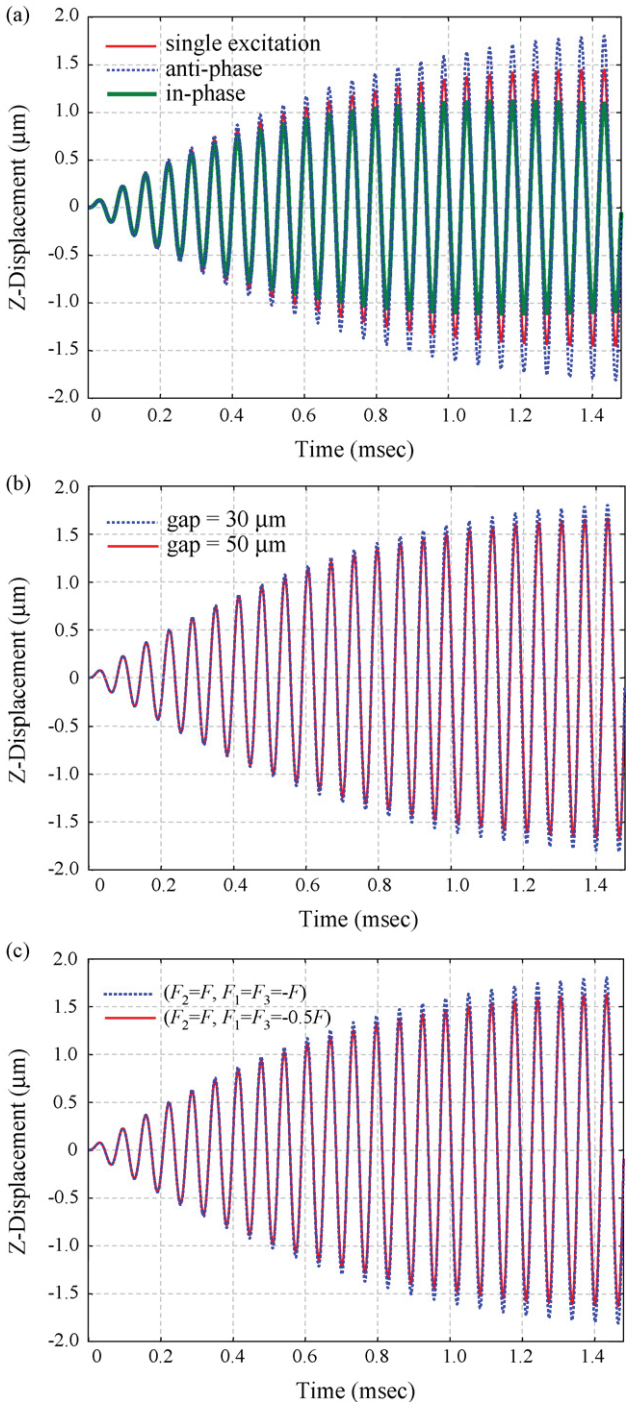

Fig. 3. The transient time response of operating-cantilever at different excitation conditions of auxiliary-cantilevers, (a) anti-phase versus in-phase excitations, single cantilever response as a reference, (b) cantilevers with different gaps, and (c) different magnitudes of excitation force on auxiliary-cantilevers.

predictions of the transient time response of operating-cantilever operated at different excitation conditions and beam array designs.

As shown in Fig. 2(b), as the excitation forces (F_1 and F_3) on auxiliary-cantilevers and the excitation force F_2 on operating-cantilever are in anti-phase ($F_1 = F_3 = -F$, $F_2 = F$), the operating-cantilever and auxiliary-cantilevers will oscillate nearly in anti-phase. The induced air-damping forces by auxiliary-cantilevers exerted on operating-cantilever are in the same moving direction of operating-cantilever, and then the net air damping of operating-cantilever will be decreased. Thus, the transient time response of operating-cantilever in anti-phase operation is larger than that in single excitation operation (without excitation of auxiliary-cantilevers: $F_2 = F$, $F_1 = F_3 = 0$) as shown in Fig. 3(a) by numerical simulation. On the other hand, when the excitation forces (F_1 and F_3) on auxiliary-cantilevers and the excitation force F_2 on operating-cantilever are in in-phase ($F_1 = F_2 = F_3 = F$), as indicated in Fig. 2(c), the operating-cantilever and auxiliary-cantilevers will oscillate nearly in in-phase. The induced air-damping forces by auxiliary-cantilevers exerted on operating-cantilever are in the opposite moving direction of operating-cantilever, and then the net air damping of operating-cantilever will be increased. Thus, the transient time response of operating-cantilever in in-phase operation is smaller than that in single excitation operation as shown in Fig. 3(a).

As shown in Fig. 1(c), the velocity of the induced air flow is related to its distance to the vibrating cantilever. In other words, the hydrodynamic coupling of micro-cantilevers is sensitive to the distance between cantilevers [20]. The simulation results in Fig. 3(b), respectively, show the transient time responses of operating-cantilever having a gap of 30 μm and 50 μm with auxiliary-cantilevers, and the operating-cantilever is oscillating in anti-phase with the auxiliary-cantilevers. It shows the operating-cantilever with a smaller gap has larger length of the transient time. Thus, the gap between auxiliary-cantilevers and operating-cantilever can be exploited to modify the quality factor of operating-cantilever.

Moreover, the magnitude of excitation forces F_1 and F_3 can be employed to modulate the vibration amplitudes of auxiliary-cantilevers, and further exploited to tune the hydrodynamic forces on operating-cantilever. Fig. 3(c) compares the transient time response of operating-cantilever in anti-phase excitation with auxiliary-cantilevers for different magnitudes of excitation forces. It shows larger excitation force ($F_1 = F_3 = -F$) has larger length of the transient time of operating-cantilever. As a result, it is easy to tune the quality factor of the operating-cantilever by varying the magnitudes of excitation forces on auxiliary-cantilevers. In short, this study experimentally investigates the hydrodynamic coupling of the micro-cantilever array to quantitatively characterize the effects of phase, gap, and force factors on the controlling of the quality factor of operating-cantilever.

According to Hosaka's theoretical model [20], the equations of motion for the dynamic system of the three micro-cantilevers in Fig. 2(a) can be expressed as:

$$\begin{cases} m_{11}\ddot{u}_1 + c_{11}\dot{u}_1 + c_{12}\dot{u}_2 + k_{11}u_1 = F_1 \\ m_{22}\ddot{u}_2 + c_{21}\dot{u}_1 + c_{22}\dot{u}_2 + c_{23}\dot{u}_3 + k_{22}u_2 = F_2 \\ m_{33}\ddot{u}_3 + c_{32}\dot{u}_2 + c_{33}\dot{u}_3 + k_{33}u_3 = F_3 \end{cases} \quad (1)$$

where u_1, u_2, u_3 are the displacements, m_{11}, m_{22}, m_{33} are the equivalent masses, c_{11}, c_{22}, c_{33} are the equivalent damping coefficients, k_{11}, k_{22}, k_{33} are the equivalent stiffnesses, and F_1, F_2, F_3 are the external forces for beam 1 (left auxiliary-cantilever), beam 2 (middle operating-cantilever) and beam 3 (right auxiliary-cantilever), respectively. The vibration of operating-cantilever induces $c_{12}\dot{u}_2$ and $c_{32}\dot{u}_2$ hydrodynamic forces on the auxiliary-cantilevers, respectively. Meanwhile, the vibration of auxiliary-cantilevers also induces $c_{21}\dot{u}_1$ and $c_{23}\dot{u}_3$ hydrodynamic forces on the operating-cantilever as well. As a consequence, the three micro-cantilevers are dynamically coupled by the air-damping c_{12}, c_{21}, c_{23} and c_{32}.

3. Experiments

The magnetic actuated micro-cantilever array shown in Fig. 4(a) was fabricated and characterized to implement the experimental investigation in this study. Fig. 4(b)–(f) shows the fabrication process steps at A–A′ cross-section indicated in Fig. 4(a). As shown in Fig. 4(b), the thermal oxide was grown on (1 1 1) single crys-

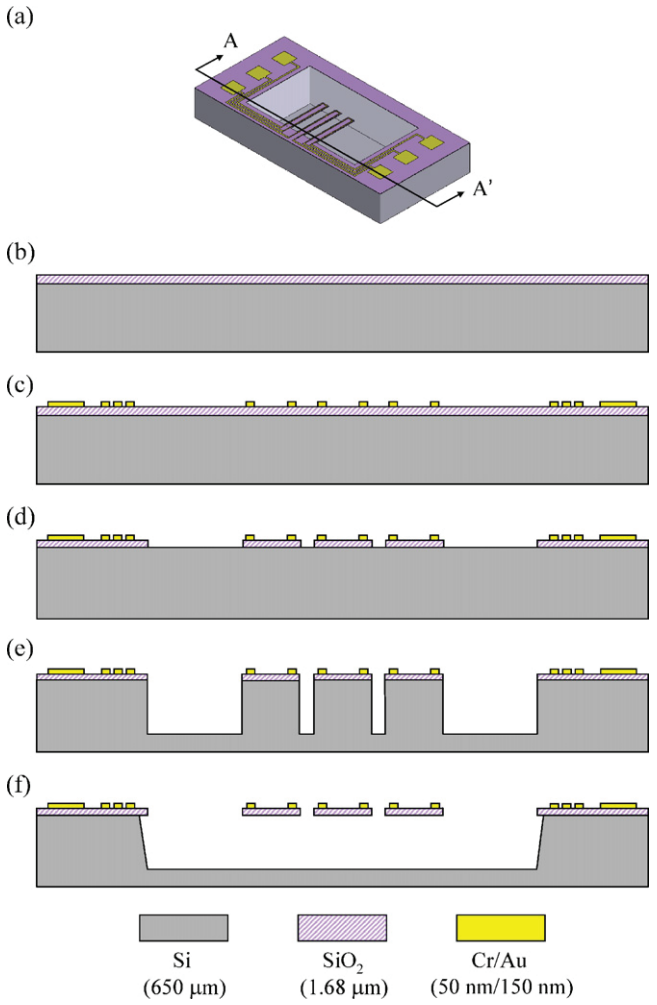

Fig. 4. The fabrication steps for micro-cantilever array, (a) the schematic diagram of test chip and the location of A–A′ cross-section to view fabrication processes, (b) grow thermal oxide, (c) deposit Cr/Au films by E-gun and patterned by lift-off, (d) etch thermal oxide by RIE to define the geometry of micro-cantilever array, (e) anisotropically etch silicon substrate by DRIE, and (f) bulk wet etching.

tal silicon wafer. As shown in Fig. 4(c), the Cr (adhesion layer) and Au films were deposited onto the SiO_2 film by E-gun evaporation and then followed by the lift-off process to pattern the metal films. Thus, the Lorentz coils and the bonding pads were defined. As illustrated in Fig. 4(d), the SiO_2 film was patterned by the photolithography and etched by reactive ion etching (RIE) to define the in-plane shape of micro-cantilevers. After that, the (1 1 1) Si substrate was anisotropically etched by deep reactive ion etching (DRIE), as shown in Fig. 4(e). This DRIE etching was also used to define the space between the suspended cantilevers and the substrate. The space of the suspended cantilevers to the substrate is 167 μm. In such space, the squeeze-film damping [22] of the cantilevers is much smaller than their viscous damping, and can be neglected. Finally, the silicon wafer was etched anisotropically by tetramethyl ammonium hydroxide (TMAH) etchant to release the micro-cantilevers, as shown in Fig. 4(f). The SEM (scanning electron microscopy) micrographs in Fig. 5 demonstrate two typical micro-cantilever arrays implemented using the process. These two micro-cantilever arrays have different gaps between the cantilevers. The cantilever array consists of three beams successfully suspended on the (1 1 1) wafer; and the bonding pads used to input the driving signals are also observed. In the experiment, the thickness of the fabricated cantilever (SiO_2) was 1.68 μm, and the thicknesses of the Cr and Au films were respectively 50 nm and 150 nm. Moreover, the zoom-in micrograph in Fig. 5 shows the close-up view of the micro-cantilevers, and the metal coils are clearly observed.

Fig. 6 shows the entire experimental setup established in this study. The test unit consists of the micro-cantilever array, the NdFeB permanent magnets (1.4 T), and a PCB (printed circuit board). The micro-cantilever array chip and the permanent magnets were fixed to the PCB. In addition, the pads on chip were wire-bonded to the PCB. The magnetic coils on auxiliary-cantilevers were connected in serial. The magnetic coils on operating-cantilever and those on auxiliary-cantilevers were connected in parallel. The variable resistors were used to control input currents of auxiliary-cantilevers and operating-cantilever. After applying current to the Au metal film, the Lorentz force introduced by the magnetic field was employed to excite the SiO_2 cantilevers. The phase and amplitude of the magnetic driving forces were easily controlled by the direction and magnitude of input current. As shown in Fig. 6, each micro-cantilever has its own driving coil and electrical routing. Thus, the dynamic response (including phase and amplitude) of each micro-cantilever can be controlled individually. In the experiment, the dynamic signal analyzer (HP 35670A) generated harmonic voltage to drive the micro-cantilever array. The dynamic response of the beam was characterized by a Laser Doppler Vibrometer (LDV, Graphtec AT-3500) system, and the measured signal was analyzed by the dynamic signal analyzer. Finally, the quality factor is extracted from the measured spectra using curve fitting based on half-power (−3 dB) method.

The driving voltage in the experiment is 20 mV. To check the parasitic driving due to electrostatic coupling or proximity effects [23] between the cantilever and the substrate underneath,

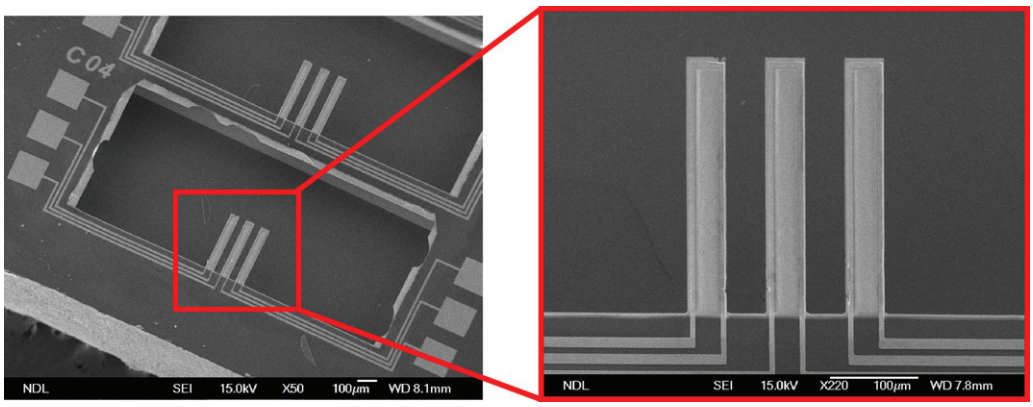

Fig. 5. The SEM micrographs of typical fabricated micro-cantilever array.

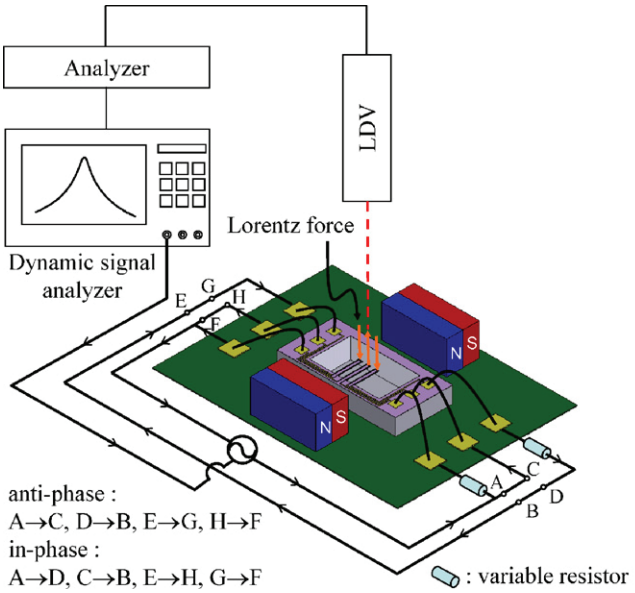

Fig. 6. The schematic diagram of the experimental setup for micro-cantilevers dynamic test and the test unit.

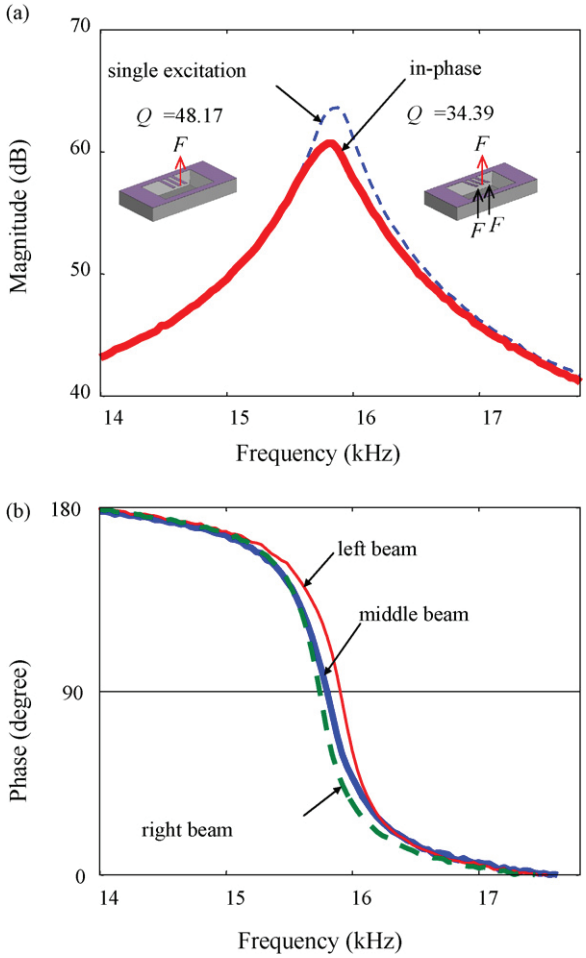

Fig. 7. The typical frequency response of micro-cantilever array at in-phase excitation: (a) magnitude, and (b) phase.

the operating-cantilever was driven by the same current level (20 mV) without magnets. The frequency response of the operating-cantilever by parasitic driving (without magnets) is much smaller than that by magnetic driving (with magnets). Thus, the parasitic driving due to electrostatic coupling or proximity effects between operating-cantilever and the substrate underneath can be neglected. Moreover, the dynamic coupling of the cantilevers through their boundary and substrate was also investigated. In such experiments, only the outside cantilevers (auxiliary-cantilevers) were excited with the same vibration amplitude; and the beams were driven at 1 atm and 70 mTorr air pressure, respectively. The dynamic response of the central cantilever (operating-cantilever) at 70 mTorr is much smaller than that at 1 atm. It shows the coupling effect of the micro-cantilever array is mainly via fluid dynamic effects.

4. Results and discussion

Fig. 7 shows the frequency response of operating-cantilever (the middle beam of the cantilever array), as the excitation forces on operating-cantilever and auxiliary-cantilevers (the left and right beams of the cantilever array) have the same magnitude ($F_1 = F_2 = F_3$) and phase. The dimension of the cantilever is 300 μm in length, 50 μm in width, and 1.68 μm in thickness, and the gap between two adjacent cantilevers is 30 μm. As indicated by the solid line in Fig. 7(a), the measured frequency response of operating-cantilever has a quality factor of $Q = 34.39$. In comparison, this study also measured the frequency response of operating-cantilever when auxiliary-cantilevers were not excited. In this case, the middle cantilever has a quality factor of $Q = 48.17$, as indicated by the dashed line in Fig. 7(a). As discussed in Section 2, the net air damping of the middle cantilever is increased at in-phase excitation of micro-cantilever array. Thus, the quality factor of the middle cantilever is decreased from 48.17 to 34.39 (−29%). The measured phase diagram in Fig. 7(b) indicates nearly in-phase between auxiliary-cantilevers and operating-cantilever. On the other hand, Fig. 8 shows the frequency response of operating-cantilever, as the excitation forces on operating-cantilever and auxiliary-cantilever have the same magnitude but 180° out of phase (anti-phase). As indicated by the solid line in Fig. 8(a), the measured frequency response of operating-cantilever has a quality factor of $Q = 58.03$. Thus, the quality factor of the middle cantilever is increased from 48.17 to 58.03 (+20%), due to the hydrodynamic coupling of cantilevers in anti-phase vibration. In addition, the measured phase diagram in Fig. 8(b) indicates the 180° out of phase between auxiliary-cantilevers and operating-cantilever.

This study also characterized the variation of quality factor of operating-cantilever with the gap between cantilevers at anti-phase and in-phase excitation. In this experiment, cantilever arrays of seven different gaps (gaps ranging from 20 μm to 80 μm) were characterized. The dimensions of the cantilevers remain 300 μm in length, 50 μm in width, and 1.68 μm in thickness. The spread of resonance frequencies between the three cantilevers in one array induced by manufacturing non-uniformity is listed in Table 1. The variations of the resonant frequencies in one array are within

Table 1
The resonance frequencies of the cantilevers measured at different micro-cantilever arrays. In these arrays, the variations of the resonant frequencies caused by the fabrication process are within ±1.8%.

Gap (μm)	Middle beam (Hz)	Right beam (Hz)	Left beam (Hz)
20	16,080	15,948	16,080
30	15,852	15,778	15,912
40	15,671	15,767	15,728
50	15,697	15,662	15,819
60	15,738	15,718	15,627
70	15,716	15,685	15,676
80	15,884	15,597	15,802

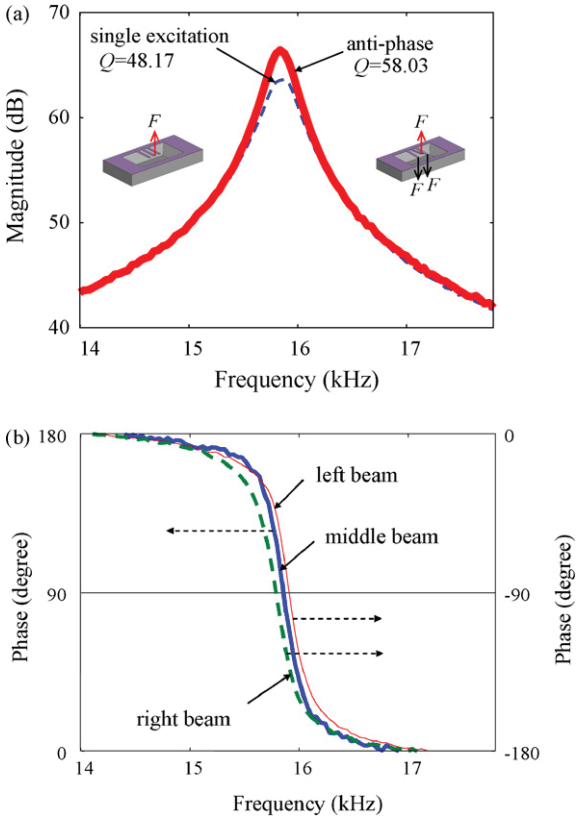

Fig. 8. The typical frequency response of micro-cantilever array at anti-phase excitation: (a) magnitude, and (b) phase.

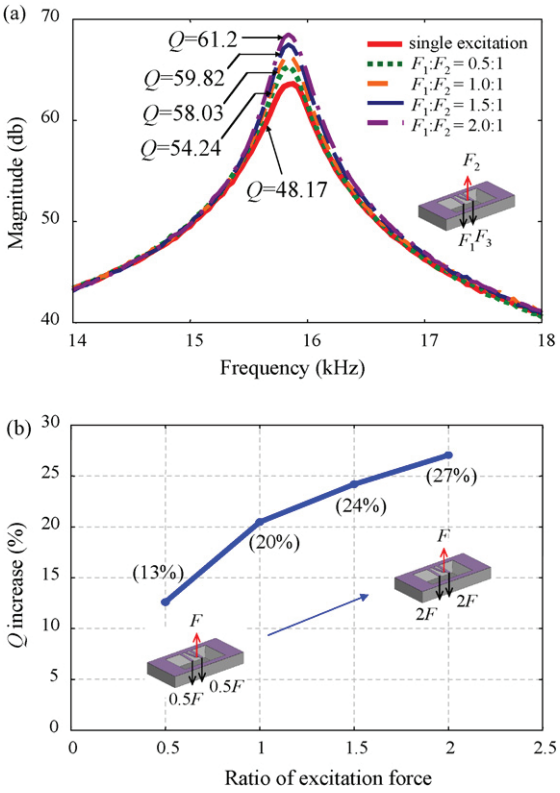

Fig. 10. Tuning the characteristics of Q by varying the loads applied on auxiliary beams, (a) frequency response of operating-cantilever, and (b) variation of Q with force ratio.

±1.8%. The excitation forces on operating-cantilever and auxiliary-cantilever have the same magnitude. As shown in Fig. 9, when the gap varying from 20 μm to 80 μm, the variation of quality factor of operating-cantilever is changed from 25% increase to 5% increase for anti-phase case, and changed from 39% decrease to 4% decrease for in-phase case. As a result, the tuning range of the quality factor is decreased when the gap between cantilevers is increased.

Moreover, the influence of excitation forces on auxiliary-cantilevers was investigated. In this experiment, the auxiliary-cantilevers and operating-cantilever with a gap of 30 μm were driven in anti-phase. The excitation forces on auxiliary-cantilevers have the same magnitude (i.e. $F_3 = F_1$, as indicated in Fig. 2). Fig. 10 shows the effect of different magnitudes of auxiliary-cantilevers excitation forces on the dynamic response of operating-cantilever. Fig. 10(a) shows the measured dynamic responses at different force ratios of F_1/F_2. Measurements show the dynamic response of operating-cantilever near the resonant frequency is especially magnified while increasing the excitation force of auxiliary-cantilevers. As shown in Fig. 10(b), when the excitation force F_1 increasing from 0.5 to 2-folds (while the force on operating-cantilever $F_2 = F$ remains the same), the quality factor of operating-cantilever increases from 54.24 (+13%) to 61.2 (+27%). As discussed in Section 2, increasing the excitation forces (F_1 and F_3) on auxiliary-cantilevers increases the induced hydrodynamic forces on operating-cantilever, and such effect is enlarged near the resonance. Thus, the magnitude of excitation force on auxiliary-cantilevers can be exploited to tune the quality factor of operating-cantilever.

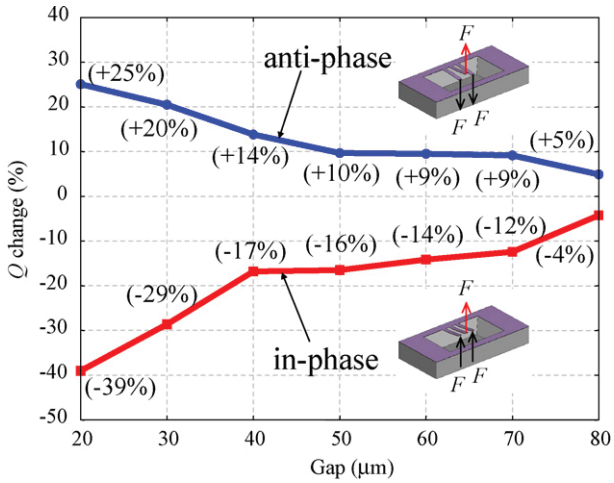

Fig. 9. Tuning the characteristic of Q by varying the gap between cantilevers.

In summary, as compared with the existing active Q-control method [17–19], the hydrodynamic coupling of micro-cantilever array approach has a smaller tuning range of quality factor. However, it provides a much simpler way to active control the quality factor of a cantilever. The complicated electronic feedback system to trace the vibration phase of the cantilever is prevented. Moreover, a cantilever with larger width could induce larger air flow force to its adjacent microstructures. Thus, the tuning range of quality factor could be further enhanced using wider auxiliary-cantilevers. Furthermore, an alternative driving method (in-phase in one of auxiliary-cantilevers and anti-phase in the other auxiliary-cantilever) would induce torsional vibration modes in the operating-cantilever, which may help to reduce the hydrodynamic damping of cantilevers working in liquids.

5. Conclusions

This study experimentally investigates the effect of controlling the dynamic response of a micro-cantilever using hydrodynamic coupling of active micro-cantilever array. The active micro-cantilever array consists of one operating cantilever and two auxiliary-cantilevers. The vibrating auxiliary-cantilevers generate hydrodynamic forces on operating-cantilever, so as to change the air damping of operating-cantilever. Thus, the dynamic response of operating-cantilever can be modified by controlling the oscillation of auxiliary-cantilevers. To implement the experimental investigation, magnetic actuated micro-cantilever arrays were fabricated and characterized. Experimental results show the quality factor of operating-cantilever can be increased or decreased by changing the phase of the excitation force on auxiliary-cantilevers. Moreover, the tuning range of the quality factor is decreased when the gap between cantilevers is increased. As gap varying from 20 μm to 80 μm, the quality factor of operating-cantilever is changed from +25% to +5% for anti-phase case, and changed from −39% to −4% for in-phase case. Additionally, the excitation force of auxiliary-cantilevers can be exploited to tune the quality factor of operating-cantilever. As the excitation force on auxiliary-cantilevers increasing from 0.5 to 2-folds, the quality factor of operating-cantilever increases from +13% to +27%.

Acknowledgements

This research is supported by the National Science Council of Taiwan under the grant of NSC-97-2221-E-492-010. The authors would like to thank the Center for Nanotechnology, Materials Science, and Microsystems of National Tsing Hua University, the NEMS Research Center of National Taiwan University, the Nano Facility Center of National Chiao Tung University, and the National Nano Device Laboratory of National Applied Research Laboratories for providing the fabrication facilities.

References

[1] R.M. Lin, W.J. Wang, Structural dynamics of microsystems-current state of research and future directions, Mech. Syst. Signal Process. 20 (2006) 1015–1043.
[2] V.T. Srikar, S.D. Senturia, Thermoelastic damping in fine-grained polysilicon flexural beam resonators, J. Microelectromech. Syst. 11 (2002) 499–504.
[3] J. Yang, T. Ono, M. Esashi, Energy dissipation in submicrometer thick single-crystal silicon cantilevers, J. Microelectromech. Syst. 11 (2002) 775–783.
[4] G. Piazza, P.J. Stephanou, A.P. Pisano, Single-chip multiple-frequency ALN MEMS filters based on contour-mode piezoelectric resonators, J. Microelectromech. Syst. 16 (2007) 319–328.
[5] C. Ziegler, Cantilever-based biosensors, Anal. Bioanal. Chem. 379 (2004) 946–959.
[6] N.V. Lavrik, M.J. Sepaniak, P.G. Datskos, Cantilever transducers as a platform for chemical and biological sensors, Rev. Sci. Instrum. 75 (2004) 2229–2253.
[7] G.Y. Chen, R.J. Warmack, T. Thundat, D.P. Allison, A. Huang, Resonance response of scanning force microscopy cantilevers, Rev. Sci. Instrum. 65 (1994) 2532–2537.
[8] S. Bianco, M. Cocuzza, S. Ferrero, E. Giuri, G. Piacenza, C.F. Pirri, A. Ricci, L. Scaltrito, D. Bich, A. Merialdo, P. Schina, R. Correale, Silicon resonant microcantilevers for absolute pressure measurement, J. Vac. Sci. Technol. B 24 (2006) 1803–1809.
[9] J.F. Vignola, J.A. Judge, J. Jarzynski, M. Zalalutdinov, B.H. Houston, J.W. Baldwin, Effect of viscous loss on mechanical resonators designed for mass detection, Appl. Phys. Lett. 88 (2006) 041921.
[10] W.Y. Shih, X. Li, H. Gu, W.-H. Shih, I.A. Aksay, Simultaneous liquid viscosity and density determination with piezoelectric unimorph cantilevers, J. Appl. Phys. 89 (2001) 1497–1505.
[11] M.R. Dokmeci, A. Pareek, S. Bakshi, M. Waelti, C.D. Fung, K.-H. Heng, C.H. Mastrangelo, Two-axis single-crystal silicon micromirror arrays, J. Microelectromech. Syst. 13 (2004) 1006–1017.
[12] W.E. Newell, Miniaturization of tuning forks, Science 161 (1968) 1320–1326.
[13] C.-M. Ho, Y.-C. Tai, Micro-electro-mechanical systems (MEMS) and fluid flows, Annu. Rev. Fluid Mech. 30 (1998) 579–612.
[14] C.-C. Cheng, W. Fang, Tuning the quality factor of bulk micromachined structures using squeezed-film damping, Microsyst. Technol. 11 (2005) 104–110.
[15] K.B. Lee, Y.-H. Cho, Electrostatic control of mechanical quality factors for surface-micromachined lateral resonators, J. Micromech. Microeng. 6 (1996) 426–430.
[16] S. Basak, A. Raman, S.V. Garimella, Hydrodynamic loading of microcantilevers vibrating in viscous fluids, J. Appl. Phys. 99 (2006) 114906.
[17] J. Tamayo, A.D.L. Humphris, A.R. Malloy, M.J. Miles, Chemical sensors and biosensors in liquid environment based on microcantilevers with amplified quality factor, Ultramicroscopy 86 (2001) 167–173.
[18] A.D.L. Humphris, A.N. Round, M.J. Miles, Enhanced imaging of DNA via active quality factor control, Surf. Sci. 491 (2001) 468–472.
[19] H. Holscher, D. Ebeling, U.D. Schwarz, Theory of Q-controlled dynamic force microscopy in air, J. Appl. Phys. 99 (2006) 084311.
[20] H. Hosaka, K. Itao, Coupled vibration of microcantilever array induced by airflow force, J. Vib. Acoust. 124 (2002) 26–32.
[21] J.-H. Lee, S.-T. Lee, C.-M. Yao, W. Fang, Comments on the size effect on the microcantilever quality factor in free air space, J. Micromech. Microeng. 17 (2007) 139–146.
[22] H. Hosaka, K. Itao, S. Kuroda, Damping characteristics of beam-shaped micro-oscillators, Sens. Actuators, A 49 (1995) 87–95.
[23] J. Malo, J.I. Izpura, Simultaneous magnetic and electrostatic driving of microcantilevers, Sens. Actuators, A 136 (2007) 347–357.

Biographies

Jiunn-Horng Lee was born in Kaohsiung, Taiwan, in 1964. He received his master degrees from the Department of Mechanical Engineering at National Cheng-Kung University, Taiwan, in 1991. He joined National Center for High-performance Computing, Taiwan, in 1991, where he is now an associate researcher. Currently he is also studying for PhD degree in Institute of NanoEngineering and MicroSystems, National Tsing Hua University, Taiwan. His research interests include computer-aided analysis of MEMS, solid mechanics and high-performance computing

Yung-Dong Lau was born in Kaohsiung, Taiwan, in 1980. He received his master degree from the Department of Mechanical and Computer-Aided Engineering, Feng Chia University in 2005. Currently he is studying for PhD degree in Power Mechanical Engineering Department, National Tsing Hua University, Taiwan. His major research interests include MEMS instrument and characterization of the mechanical properties of thin films

Chih-Min Yao was born in Hsinchu, Taiwan, in 1964. He received his master and PhD degrees from the Mechanical Engineering Department of National Taiwan University, Taiwan in 1988 and 1994, respectively. He joined National Center for High-performance Computing, Taiwan in 1994, where he is now a researcher. His research interests include computer-aided analysis in MEMS, solid mechanics and multi-body dynamics, as well as computational biomechanics

Weileun Fang was born in Taipei, Taiwan, in 1962. He received his PhD degree from Carnegie Mellon University in 1995. His doctoral research focused on the determining of the mechanical properties of thin films using micromachined structures. In 1995, he worked as a postdoctoral research at Synchrotron Radiation Research Center, Taiwan. He joined the Power Mechanical Engineering Department at the National Tsing Hua University (Taiwan) in 1996, where he is now a Professor as well as a faculty of NEMS Institute. From June to September 1999, he was with Prof. Y.-C. Tai at California Inst. Tech. as a visiting associate. He served as the TPC of IEEE MEMS'04 '07 and '10, the regional TPC of Transducers '07, and the EPC of Transducers '09. He is now on the Editorial Board of *JMM*, and the Associate Editor of *JM3*. He has established a MEMS testing and characterization lab. His research interests include MEMS with emphasis on microfabrication/packaging technologies, CMOS MEMS, microoptical systems, microsensors and actuators, and the characterization of the mechanical properties of thin films.